MAGNETOHYDRODYNAMICS Vol. 45 (2009), No. 1, pp. 25–42

MODEL EXPERIMENTS ON MACROSCOPIC THERMOELECTROMAGNETIC CONVECTION

X. Zhang[1], *A. Cramer*[1], *A. Lange*[2], *G. Gerbeth*[1]

[1] *Forschungszentrum Dresden–Rossendorf, Institute of Safety Research, P.O. Box 510119, 01314 Dresden, Germany*

[2] *Institute of Surface and Manufacturing Technology, Technische Universität Dresden, 01069 Dresden, Germany*

The interaction between a thermoelectric current and an imposed magnetic field may produce thermoelectromagnetic convection (TEMC). In the present paper, an experimental study on TEMC in a generic configuration is reported. While the necessary temperature gradient $\operatorname{grad} T$ in a square box was accomplished by heating and cooling of two opposing side walls, respectively, utilising a massive nickel plate for the bottom of the electrically conducting container established a material discontinuity with respect to the liquid metal layer. Primarily, such a jump in the related Seebeck coefficient non-parallel to $\operatorname{grad} T$ is a pre-requisite for the existence of a thermoelectric current. The second condition for TEMC, which is a non-vanishing curl of the Lorentz force, was fulfilled using a permanent magnet producing an inhomogeneous magnetic field.

Ultrasonic Doppler velocimetry was used to quantify the TEMC flow field. The measurements demonstrate that even a moderate temperature difference can produce a distinct convection. Locating the magnet, the direction of magnetization of which was parallel to $\operatorname{grad} T$, close to either side wall produced a single vortex spreading throughout the entire box. Moving the magnet to the centre led to a modified distribution of the magnetic field, which, in turn, altered the flow pattern. A convective pattern consisting of four vortices developed and the velocity fluctuations were intensified. The numerical results for the distribution of the magnetic field in the presence of the ferromagnetic bottom support the experimental findings.

PACS number(s): 47.65.-d, 52.30.Cv

1. Basics of thermoelectromagnetic convection. Thermoelectromagnetic convection (TEMC) is based on the principle that a temperature gradient $\operatorname{grad} T$ generates an electro-motive force (e.m.f.). To derive the relevant relations, three pieces of wire from two different materials, say α and β, in a configuration of a sequence α–β–α are considered. In the isothermal case, the voltage drop between both ends of this configuration is zero. If one of the junctions is heated to T_h and the other one is cooled to T_c, a difference in the electric potential U can be measured. U depends on the temperature difference between both junctions and is otherwise determined by the absolute thermoelectric powers S_α and S_β of the respective materials. Obviously, such a configuration is a thermocouple and the coefficient of thermoelectric power $S_\beta - S_\alpha$ is commonly known as the (relative) Seebeck coefficient. Independent of the ambient temperature T_a, the e.m.f. is given by

$$U = S_\alpha(T_\mathrm{a} - T_\mathrm{h}) + S_\beta(T_\mathrm{h} - T_\mathrm{c}) + S_\alpha(T_\mathrm{c} - T_\mathrm{a}) = (S_\beta - S_\alpha)(T_\mathrm{h} - T_\mathrm{c}). \quad (1)$$

Closing the loop by joining both ends will result in a thermoelectric current $\mathbf{j}$. As we shall see below, an additional pre-requisite has to be fulfilled when move from the simple 1D alignment to a realistic 3D configuration in order to have a thermoelectric current circulating in the system. This condition is that the gradients of S and T are not parallel. Application of a magnetic field to such a

system, however, may produce a thermoelectromagnetic body force **f** and, in the case that one of the thermoelectric *limbs* is liquid, a relevant flow in the melt.

Albeit thermoelectric pumps have been developed and patented starting in the middle of the 1950's [1–4], the pioneering systematic study on TEMC was performed by Shercliff [5]. He generalised the Ohm's law for conducting liquids by introducing a term for the e.m.f.

$$\frac{\mathbf{j}}{\sigma} = \mathbf{E} + \mathbf{v} \times \mathbf{B} - S \operatorname{grad} T, \tag{2}$$

where σ, $\mathbf{v}$, $\mathbf{E}$, and $\mathbf{B}$ are the electric conductivity of the liquid metal, the velocity at which it moves, and the electric and magnetic fields, respectively. In a system, in which $\mathbf{v} \times \mathbf{B}$ is negligibly small and $\mathbf{E}$ is irrotational, the latter implying $\mathbf{E} = -\operatorname{grad}\varphi$ with the electric potential φ, Eq. (2) simplifies to

$$\frac{\mathbf{j}}{\sigma} = -\operatorname{grad}\varphi - S \operatorname{grad} T. \tag{3}$$

Considering any arbitrary temperature distribution in a medium of uniform composition in Eq. (3) shows that no current passes because $S \operatorname{grad} T$ is also irrotational. This is due to S being a function of T only, a consequence of which is that $\operatorname{grad} S \times \operatorname{grad} T$ vanishes. At this stage, it is returned to the pre-requisite mentioned above: in order to have thermoelectric current flowing, the vectors $\operatorname{grad} S$ and $\operatorname{grad} T$ must not be parallel. This is, in general, accomplished by a spatially varying composition.

This work is concerned with the case that was termed by Shercliff as "the extreme case when the composition and S vary discontinuously across an interface along which T varies." Ignoring the dependence of S on T within either the medium is justifiable here although, in fact, $\partial S/\partial T$ may become pronounced as it is well known for some semiconductor melts. Again following Shercliff, the experimental setup of a liquid metal flowing in a differentially heated electrically conducting container might be regarded as an embodiment of what he proposed theoretically as an idea for "thermoelectric magnetohydrodynamics in metallurgy."

It is instructive to have also the point of view of electric engineering by analogy with Eq. (1). A two-dimensional system according to Fig. 1 is considered. No e.m.f. is assumed to be generated by the isothermal copper walls in combination with the

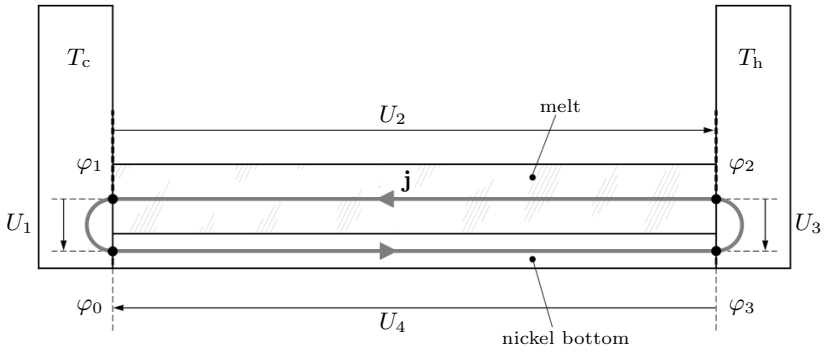

Fig. 1. Sketch of the thermoelectric current **j** in a horizontally infinite (perpendicular to the paper plane) configuration with differently heated side walls. The origin of **j** is explained in the narrative.

melt or the nickel bottom, respectively so as to be left with the melt and bottom layers, the left side of which is kept at T_c and the right one at T_h. At four points, two at the cold wall and the other two at the hot wall, from each pair of which one point lies in the domain of the melt and the second at the nickel bottom, the electric potential is considered. $U_\mathrm{n} = \varphi_\mathrm{n} - \varphi_{\mathrm{n}-1}$, where $\varphi_4 = \varphi_0$ denotes the differences between these points. According to the Kirchhoff's voltage law, the sum over the loop has to be zero

$$-U_1 + U_2 + U_3 + U_4 = 0, \tag{4}$$

with the negative value of U_1 owing to the direction of the arrows sketched in Fig. 1. The horizontal voltage drops across the layers are given by

$$U_2 = (T_\mathrm{h} - T_\mathrm{c})\, S_\mathrm{melt} - IR_\mathrm{melt} \tag{5}$$

$$U_4 = (T_\mathrm{c} - T_\mathrm{h})\, S_\mathrm{bottom} - IR_\mathrm{bottom}, \tag{6}$$

where I is the integral current corresponding to its density j, and R is the electric resistance corresponding to the reciprocal of the electric conductivity σ. The diminution of the *terminal voltage* U due to the electric current pass is the analogue to Eq. (3).

At first sight, the three equations (4)–(6) for four unknown voltages pose an under-determined problem. Closer examination shows that the information is sufficient for the purpose here. Inserting Eq. (5) and (6) in Eq. (4) yields

$$U_3 = U_1 + (T_\mathrm{h} - T_\mathrm{c}) \cdot (S_\mathrm{bottom} - S_\mathrm{melt}) + I(R_\mathrm{melt} + R_\mathrm{bottom}). \tag{7}$$

Note that the term $2R_\mathrm{sidewall}$ is neglected because of the resistance of the massive copper walls being very small compared to either R_melt or R_bottom. For the same reason, in combination with the electrotechnical Ohm's law $U = RI$, also U_1 and U_3 may be neglected. In this way, one arrives at

$$I = \frac{\Delta S \Delta T}{R_\mathrm{melt} + R_\mathrm{bottom}}, \tag{8}$$

where $\Delta S = S_\mathrm{melt} - S_\mathrm{bottom}$ and $\Delta T = T_\mathrm{h} - T_\mathrm{c}$. The simple Eq. (8) allows estimating the circulating current I.

2. A survey on the previous literature. Having considered the basics of TEMC so far, it deems worthy to dip into some of the previous work done in the field. Thermoelectric pumps might be assessed to be the state of the art in the development of nuclear reactors and space flights [6, 7]. So to speak, they are at a stage of optimisation and subject of ongoing research as can be seen from the publication date of [7].

Seemingly, most of the scientific investigation was done on crystal growth systems. In [8], Bridgeman growth under the influence of a uniform axial field B was studied numerically. The system under consideration was simplified to the model case of a planar interface, parabolic temperature gradient at that interface, and the physical properties within the melt and crystal being independent of temperature. Since the analysis is carried out in dimensionless form, it is most instructive to have a look at the discussion, in which the authors refer to a particular substance. For $\Delta T = 10\,\mathrm{K}$, $\Delta S = 10\,\mu\mathrm{V/mK}$, and a Hartmann number $\mathrm{Ha} = BR(\sigma/\mu)^{1/2}$ of 700, the characteristic velocities become $U_\mathrm{a} = 2 \cdot 10^{-3}\,\mathrm{m/s}$ for the azimuthal and $U_\mathrm{m} = 7.6 \cdot 10^{-7}\,\mathrm{m/s}$ for the meridional component. $R = 1\,\mathrm{cm}$ is the radius and μ is the dynamical viscosity. $\mathrm{Ha} = 700$ indicates a quite strong magnetic

field, which is compared to the experimental work in [9], where striations in silicon crystals grown by the floating zone process were found. There, it is argued that the striations are produced by TEMC. Parameters in [9] are provided as follows: $R = 4\,\mathrm{mm}$, $\Delta S = 10\,\mu\mathrm{V/mK}$, $\Delta T = 10\,\mathrm{K}$, Ha = 300, the latter being equivalent to 2 T. The characteristic velocities $U_\mathrm{a} = 3.75 \cdot 10^{-3}\,\mathrm{m/s}$ and $U_\mathrm{m} = 1.8 \cdot 10^{-6}\,\mathrm{m/s}$ differ not that much from those found in [8].

In order to interpret the results in the framework of potential application of TEMC to metallurgical processes, it is notable that relatively strong magnetic fields are needed. Some of the authors of [9] investigated the same system under the influence of weak magnetic fields, and have not found an indication of the presence of thermoelectric effects [10]. In [11], the germanium-silicon system in vertical Bridgman growth was studied, again with a strong axial field of up to 5 T being applied. Usually, such strong fields were employed to obtain a pure diffusion-controlled growth, but the outcome of the experiments was the observation of a strong microsegregation in the range of field strength from 0.5 to 4 T. This microsegregation, which was strongest at $B = 2\,\mathrm{T}$, was attributed to TEMC.

A strength of B of the order of a few Tesla, as it is common for the applications in crystal growth discussed above, would hardly be affordable in metallurgical processes. Moreover, melt velocities in the range of less than mm/s would not suffice to manage metallurgical tasks such as stirring, pumping and homogenisation. This has to be regarded in conjunction with the extremely high differential Seebeck coefficient $\Delta S = 10\,\mu\mathrm{V/mK}$ reported in [8] and [9]: it is about 3 orders of magnitude higher than what is achievable with pure metals and metallic alloys. That said, the question might be posed how to accomplish an even stronger flow with weaker magnetic fields. The Ohm's law, in its elementary form used in electric engineering $U = R \cdot I$, gives the answer: whatever voltage U, no significant current I passes if the resistance R is high; and the solidified crystal is an extremely poor electric conductor.

For comprehensiveness, it is noted that thermoelectromagnetic effects may also play a role on the microscopic scale. In [12], a modification of interdentritic convection during directional solidification is reported when a uniform magnetic field is applied. Theoretical investigation and experiment showed that the thermoelectric effect might be used to either brake or enhance the interdentritic convection. A recent experiment [13] demonstrated the influence of the thermoelectromagnetic effect on the cellular morphology in the mushy zone during directional solidification of AlCu alloys and, on the macroscopic scale, a modification of the solid-liquid interface shape. Again, quite strong magnetic fields had to be applied in order to attain a distinct effect.

Shercliff's proposal to employ the thermoelectric effect in metallurgy was, to the best of our knowledge, for the first time taken up by Gorbunov [14]. Albeit his work was motivated by crystal growth, he used, besides, other containers, also one made of copper. With the latter, the severe restriction on the strength of the thermoelectrically generated current, which is caused by the presence of the electrically poor conducting crystal in the current paths in [9–11], is removed. Gorbunov's experiments on InSb in quartz and graphite crucibles at higher temperature differences are not recalled here since they are indeed related primarily to crystal growth. Although being the minor part of his work, it is restricted to the investigations with the cylindrical copper container, the radius of which is 100 mm and therewith large compared to the crystal growth configurations considered so far. A temperature difference up to 200 K was applied between a circular bottom heater at half the container radius and the water-cooled lateral wall. The magnetic field was always uniform, directed axially, and variable in strength up to 200 mT.

A 25 mm thick layer of GaInSn covered with diluted acid on top was used. The acid served two purposes: it protected the liquid alloy from oxidation and, while carrying finely suspended particles, allowed a qualitative visualisation of the flow at the surface. Although vertical temperature gradients exist in such a system, they will not generate thermoelectric current in this direction for reasons given in Section 1. The radially directed $\mathbf{j}$ and the vertically applied $\mathbf{B}$ thus have to result in an azimuthal thermoelectromagnetic body force realising a rotatry stirring: a rotation of the melt layer with up to 3 rpm was observed. It is worth noting that the highest velocities were not detected at the maximum field strength. To the best to be read off Fig. 1 in [14], the maximum rotation rate was achieved for about 50 mT. Gorbunov explains this pronounced maximum by the damping effect of the static magnetic field counteracting TEMC.

Studies on TEMC in geometries other than cylinders with the magnetic field applied in the axial direction are rare. In [15], the case of liquid metal contained in an electrically conducting cubic box was studied numerically. Two of the opposing side walls were heated and cooled, respectively, while the other four walls were assumed as ideal thermal insulators. The electric conductivity was the same for all six walls and the liquid metal. The main finding of the numerical study is that TEMC dominates the inherently present buoyant convection in such a system for Rayleigh numbers up to $\mathrm{Ra} = 10^5$.

3. Motivation. Thermoelectric effects widely exist in industrial applications. The present work originates from the idea of contactless control of the flow in the melt pool during laser beam welding. Despite the small size of typically $1\,\mathrm{mm}^3$ of the weld pool, velocities of the order of m/s are observed. On such length scales, capillary forces dominate buoyancy and the Marangoni convection becomes very strong because of the large temperature gradients. The latter may become extremely high: at the point of impingement of the laser beam the temperature reaches the boiling point of the metal to be welded, whereas it drops below the melting point at half the diameter of the weld pool away. One is concerned with a few thousand degree per millimetre. The presence of such strong $\operatorname{grad} T$ may also be a reason of a significant thermoelectric current distribution in the weld pool. Discontinuities of the corresponding Seebeck coefficients may be expected between the solidified seam material and the melt, and also between the base material and the melt. Further, the material with a significantly different Seebeck coefficient attaching the base material may have a thermoelectric current circulating through the weld pool, thereby making available an efficient means of process control.

The problem in the interpretation of the outcome of welding experiments is the complexness of the system. Only the shape of the finally solidified weld seam is available for diagnostics. The path of the thermoelectrically generated current, and all the more the TEMC that had been created by the applied magnetic field, might only be guessed at hand of general arguments. What is badly needed are meaningful model experiments, which, most desirably, are of some generic kind. As available experiments are limited to the cylindrical geometry with an axially directed homogeneous field, an alternative was sought. In order to have $\operatorname{rot}(\mathbf{j} \times \mathbf{B})$ not vanishing, either $\mathbf{j}$ and/or $\mathbf{B}$ must be inhomogeneous. Gorbunov [14] investigated the case of a homogeneous field imposed on an inhomogeneous current distribution. The present study is devoted to the interaction of a homogeneous current with an inhomogeneous magnetic field, so the experiments are complementary.

The remainder of the paper is organised as follows. Section 4 describes the experimental setup. Experimental results are presented and discussed in Section 5.

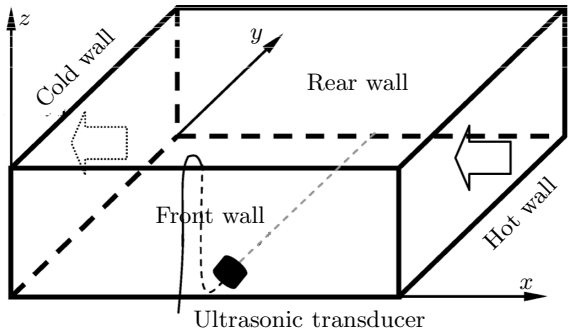

Fig. 2. Scheme of the experimental setup. A small ultrasonic transducer is located inside the liquid metal to avoid attenuation of the acoustic beam that otherwise would occur while passing the massive copper walls. The arrows indicate the direction of the heat flux.

Two different flow regimes developed in dependence on the corresponding distribution of the magnetic field are analysed. Finally, Section 6 provides a summary and points out future work on TEMC yet under consideration.

4. Experimental setup. From what is learned in Section 1 and decided thereupon in Section 2 at hand of existing work in the field, the task formulation was to accomplish a marked TEMC based on an inhomogeneity of the magnetic flux density **B**. Because of the availability of strong cobalt-samarium magnets, the demand of an inhomogeneous field is easily fulfilled using a permanent magnet made of such material having a size adapted to the dimensions of the container. The bar magnet was 50 mm in length, 20 mm in height and 8 mm in width. With the direction of magnetisation along the shortest side, measurements of the flux density produced at the surface of the magnet resulted in about 270 mT. This corresponds to a remanence of 1.1 T calculated numerically from the measurements. The experimental setup is shown in Fig. 2. Sizes of the container are length = width = 15 cm and height = 6 cm. All four side walls were made from copper plates, the relevant electric properties of which are $\sigma_{\mathrm{Cu}} = 5.96 \cdot 10^7 (\Omega\mathrm{m})^{-1}$ and $S_{\mathrm{Cu}} \approx 2\mu\mathrm{V/K}$ at room temperature. In order to create the temperature gradient within the electrically conducting fluid, one of the side walls was heated electrically and the opposing wall was cooled by water at a high flow rate. The decision for the wall material was, in parts, motivated by the high thermal conductivity, which approximates best what is commonly referred to as isothermal in the case of any heated or cooled wall.

As, for metals, thermal and electric conductivities are closely related via the Wiedemann–Franz's law, the high σ of copper is not optimal with respect to have the electric current passing mainly through the melt. In a manner of speaking *parasitic* by-passes are established with the non-isothermal (front and rear, c. f. Fig. 2) walls. It would have been possible to replace them by electrically non-conducting ones. If higher temperatures are a matter, glasses exist that can be used even in excess of 1000 °C, thus being comparable to copper. What is good in the laboratory is, however, not necessarily desirable in industrial practice. If there is a freedom to employ electrically conducting containers in a metallurgical process for TEMC stirring, these should be producible as easily as possible. Instead of sealings being required in the example with the glass walls, most probably all joints should preferably be weldable and the four side walls should be made of the

same material. So it made sense to deal with a potential industrial configuration, yet at the stage of laboratory experiments. If TEMC stirring shows up to work in a downgraded setup with loss of current, it will work more than ever in an optimised configuration. In order to curtail the current losses, the thicknesses of the front and rear walls are reduced to 5 mm. The widths of both isothermal walls are 20 mm allowing insertion of powerful heating cartridges and drilling of cooling channels for high flow rate, respectively.

For the reason of having a high difference in the Seebeck coefficient, nickel was chosen as the bottom material having the relatively high thermoelectric power of $S_{\mathrm{Ni}} = -15\mu\mathrm{V/K}$ at 55 °C [16]. It has to be acknowledged that this idea is not new. Already more than a decade ago, Bojarevičs used a cobalt plate for the bottom in a setup similar to that of Gorbunov in [14] and observed a strong rotary stirring [17]. The thickness of a bottom plate of 3 mm is sufficient to keep the Ohmic losses small thanks to the electric conductivity $\sigma_{\mathrm{Ni}} = 1.44 \cdot 10^7(\Omega\mathrm{m})^{-1}$, which is significantly higher than that of the liquid metal. The ternary alloy GaInSn was chosen as the melt under investigation for several reasons. Firstly, it is liquid at room temperature ($T_{\mathrm{melt}} = 10°\mathrm{C}$) and thus convenient to use. Secondly, GaInSn has a relatively high electric conductivity ($\sigma_{\mathrm{GaInSn}} = 3.27 \cdot 10^6(\Omega\mathrm{m})^{-1}$) among the low melting point alloys, thus rendering the Ohmic losses fairly small. Thirdly, thermo-e.m.f. data found in the literature suggest that the actual value differs not that much from that of the copper walls. Because the relatively small absolute values scatter about zero, the thermoelectric power of GaInSn was re-measured [18]. From the data supplied in Fig. 3, a value of $S_{\mathrm{GaInSn}} \approx -0.55\mu\mathrm{V/K}$ is to be read off. The TEMC in the experiments of Gorbunov was born of the difference $S_{\mathrm{Cu}} - S_{\mathrm{GaInSn}} \approx 2.5\mu\mathrm{V/K}$. This value might not be termed negligible, but it is small compared to $S_{\mathrm{Ni}} - S_{\mathrm{GaInSn}}$. If the driving force of TEMC is mainly located at one interface, the outcome of the experiments is much easier to interpret.

Prior filling the container with GaInSn alloy, the solid walls were pre-amalgamated. For that, a relatively strong hydrochloric acid was used in combination with emery wool. A droplet of the melt was rubbed across the metallic surfaces

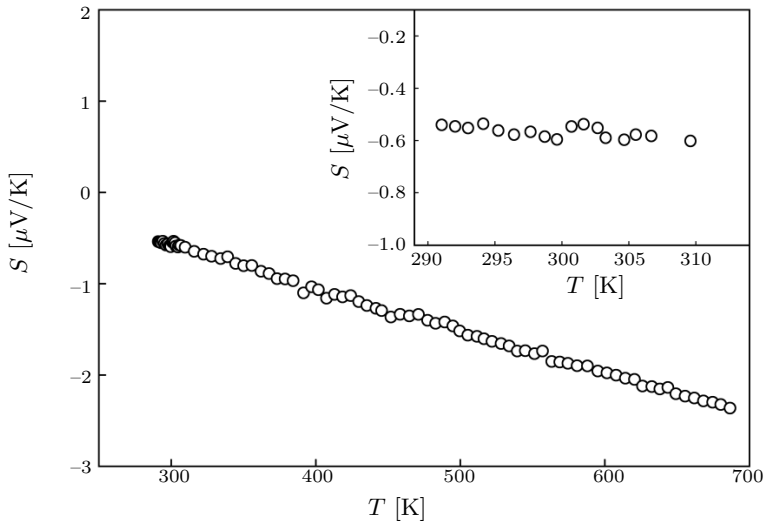

Fig. 3. Thermoelectric power of the alloy GaInSn. The relevant temperature range, within which the experiments were performed, is magnified in the upper right sub-panel. Data are communicated in [18].

until it completely wetted the solid. As this is necessary to have a uniform heat flux at the isothermal walls, it is even more important to ensure a good electric contact at the bottom. To protect the liquid alloy from too heavy corrosion, a thin layer of tartaric acid ($C_4H_6O_6$) covered the melt on top. The thickness of the GaInSn layer was kept small, being thin enough to reduce buoyant convection, but thick enough to immerse a sensor for flow measurements completely. A good compromise was 15 mm. Besides observing the motion at the melt surface, local flow measurements were performed. An ultrasonic Doppler velocimeter (UDV; model DOP2000, Signal Recovery, Lausanne/Switzerland) was used to acquire instantaneous velocity profiles along the ultrasonic beam. The principle of operation of UDV is the pulsed echo technique [19]: a time of flight measurement of an ultrasonic burst determines the location of a scattering particle within the fluid, and the difference in time of flight measurements for consecutive bursts is a measure for the velocity of the particle travelling together with the fluid. The feasibility of liquid metal local flow measurements, in particular, for recirculating flows of the GaInSn under investigation in the present work was demonstrated in [20].

5. Results and discussion. At first, the negligibleness of $\mathbf{v} \times \mathbf{B}$ made in Section 1 should be checked for the actual experimental conditions. Therefore, characteristic values of the velocity and the magnetic field have to be known. The latter may be easily calculated or measured. Numerical simulations were performed using the commercial solver Maxwell (Ansoft Corp.). Figs. 4 and 5 show that $\mathbf{B}$ is almost perpendicular to the bottom at least within the lower part of the metallic melt layer, as expected because of the ferromagnetic nickel. For an order of magnitude estimation of the $\mathbf{v} \times \mathbf{B}$ term, it is thus sufficient to restrict to B_z, while ignoring the horizontal components. For both configurations, one of which is where the magnet is located at the cold wall with its direction

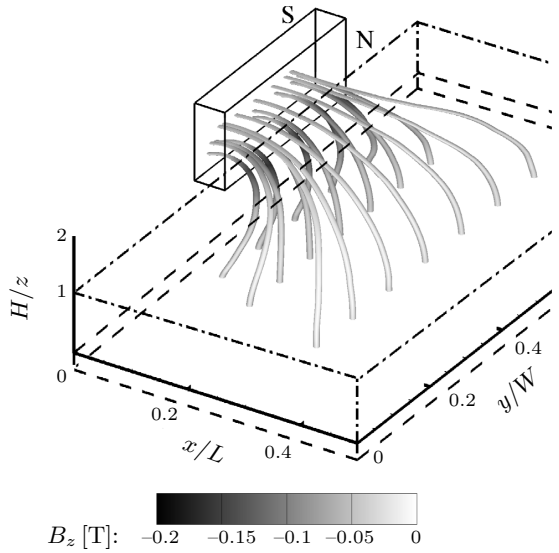

Fig. 4. Visualisation of the field of the permanent magnet in the case of the north pole directed toward the container inside. The tubes are in alignment with the direction of the vector of magnetic flux density $\mathbf{B}$, and their shading corresponds to the strength of the vertical component B_z. Geometric dimensions, in particular, the thicknesses are indicated by dashed (nickel bottom) and dash-dotted (melt) lines, respectively.

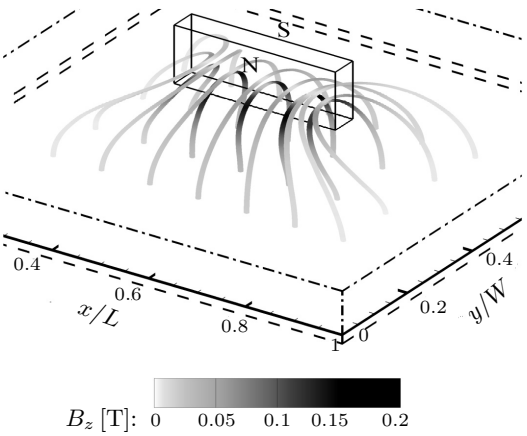

Fig. 5. Visualisation of the field of the permanent magnet in the case of the magnet located 5 mm above the centre of the liquid metal layer. For a description of the meaning of the flux tubes see Fig. 4. Due to the reason having a grey-scale presentation, the absolute value of B_z is depicted. The values of the tubes originating from the north pole are negative, and of those originating from the south pole are positive.

of magnetisation perpendicular to the wall (Fig. 4) and the other is where the magnet is moved to the centre, while it is horizontally rotated by 90 ° (Fig. 5), the measurements agreed nicely with the results of numerical simulations. A 3-axis Gauss meter (Lakeshore, model 460 with 3D sensor MMZ-2512-UH) was employed in acquiring the data; B_z was found to be up to 30 mT directly below the magnet within the melt layer decreasing rapidly with the increasing horizontal distance from the magnet, and the horizontal components of $\mathbf{B}$ were indeed very small. A characteristic velocity $\mathbf{v}$ was defined from UDV flow measurements applied to the natural convection being present in the container when the isothermal walls were heated and cooled, respectively. The buoyant convection in the box should consist of a single roll. Liquid metal rises in front of the hot wall, flows at the surface to the cold wall, descends there, and finally moves back at the bottom toward the hot wall. As verified by UDV, the velocity in the y-direction was zero everywhere, except in the close vicinity of the front and rear wall, the measured velocity sections along x did not vary with the measuring position y. Local values of v_x were in the range up to 5 mm/s at the maximum possible temperature difference of 50 K, and thus limited the value of the $\mathbf{v} \times \mathbf{B}$ term to the order of 350 μV/m. The corresponding gradient of the thermo-e.m.f. for the differential Seebeck coefficient $\Delta S = S_{\mathrm{GaInSn}} - S_{\mathrm{Ni}} = 14.45\,\mu\mathrm{V/K}$ and the same ΔT is 4.8 mV/m. Thus, the $\mathbf{v} \times \mathbf{B}$ term owing to the buoyant convection may be assumed negligible against the e.m.f. for being an order of magnitude smaller. Even the influence of $\mathbf{v} \times \mathbf{B}$ due to the TEMC exhibiting significant higher velocities is limited to, say, 30 %.

Next to be checked is whether the TEMC to be expected will dominate the intrinsic natural convection, or whether it might be only of subordinate importance. Buoyancy is governed by the Grashof number

$$\mathrm{Gr} = \frac{\beta g \Delta T l^3}{\nu^2}, \tag{9}$$

where $\beta = 1.32 \cdot 10^{-4}\,\mathrm{K}^{-1}$ is the thermal expansion coefficient, g is the acceleration of the free fall, $\nu = 3.4 \cdot 10^{-7}\,\mathrm{m}^2/\mathrm{s}$ is the kinematical viscosity, and l denotes the characteristic length of the system. Insertion of the melt layer thickness of 15 mm

for the characteristic length in Eq. (9) yields $\mathrm{Gr} = 1.89 \cdot 10^6$. It is instructive to contrast this value with the situation investigated in [15]. There, the authors considered the Rayleigh numbers up to 10^5. Using the relation $\mathrm{Ra} = \mathrm{Gr} \cdot \mathrm{Pr}$, where $\mathrm{Pr} = \nu/\chi$ is the Prandtl number, allows a direct comparison. The high thermal diffusivity of the GaInSn melt $\chi = 1.87 \cdot 10^{-5}\,\mathrm{m/s^2}$ results in the typical low Prandtl number 0.019 of liquid metals, and the Rayleigh number for the present setup becomes $3.5 \cdot 10^4$. Since the TEMC, the more so as originating from end effects only, dominates buoyancy in [15], the even lower Ra here indicates that the chosen thickness of the melt layer is small enough to ensure prevailing TEMC. Gorbunov [14] introduced the dimensionless number

$$\mathrm{Te} = \frac{\sigma \Delta S B \Delta T l^2}{\rho \nu^2} \tag{10}$$

for the relative strength of TEMC. With the density $\rho = 6360\,\mathrm{kg \cdot m^{-3}}$, one gets $\mathrm{Te} = 2.42 \cdot 10^7$. The ratio Te/Gr becomes about 13, which again justifies the neglect of natural convection.

Prior going into the details of the measurements, it is examined what might be expected from the thermoelectric effect in terms of fluid velocities. Straightforwardly, from what is analysed immediately above, the ratio of $\mathrm{Te/Gr} \approx 13$ implies much higher velocities than those measured by UDV when the magnetic field was not applied. On the other hand, such ratios must not be regarded as factors of proportionality. Scaling laws are far beyond the scope here and it is just mentioned that in the case of turbulent natural convection the velocity scales are $v \propto \sqrt{Gr}$. One may estimate the electric current for the 2D case by the order of magnitude at hand of Eq. (8) resulting in about $18\,\mathrm{kA/m^2}$. The corresponding Lorentz force density $f = j \cdot B = 528\,\mathrm{N/m^3}$ is quite high. There are hardly data on force densities published, so a comparison is difficult. In [21], force densities smaller than an order of magnitude are reported, which drive flows in the range of cm/s. Again, on the other hand, it is to be obeyed that the force in [21] spreads over the entire volume, whereas here it is restricted to the small region below the vicinity of the permanent magnet. One may sum up so far that a turbulent TEMC of the order of few cm/s in velocity is indicated.

Another consideration deems necessary, which concerns the actual 3D character of the experiment. The derivation of Eq. (8) from the Kirchhoff's law in Section 1 relies on a 2D configuration. Also, the estimation of the integral current in the paragraph above is based on such an idealisation. The description of the experiment in Section 4, however, evinces that the configuration under consideration is certainly removed from the simple 2D case for the reason of having electrically high conducting walls (front and rear) in the direction of the temperature gradient. This poses the question, to which extent the distribution of the thermoelectric current, and in turn the TEMC, is affected. Thus, it would be desirable to have a Kirchhoff's law also for the direction perpendicular to $\mathrm{grad}\,T$. Unfortunately, what holds for the x-direction continues to be true for the y-direction: here, the current distribution is influenced by the isothermal (hot and cold) walls, which are even thicker. This means, as it is mostly the case in physical modelling, that it is not possible to describe the configuration by a system of Kirchhoff's laws analytically. Instead of a therefore unconditionally required full 3D numerical simulation, which is beyond the scope of the present paper, it is put forward by arguments that, at least, the resulting TEMC is only somewhat affected by the presence of the copper walls.

Consider the whole area of contact between the Ni bottom and the melt being composed of infinitely small areas. Each of these small elements produces a

thermo-e.m.f. in the x-direction. Whether the current distribution created by any element is influenced by the copper walls depends on its distance to those walls. From the point of view of electric engineering, the copper wall is a resistor switched in parallel to the internal resistance of the element. The resistivity of the copper may even be neglected, the resistance of the *by-pass* is, primarily, determined by the ratio of the distance of the element to the wall to its own size. Seeing that a length of 5 cm of the magnet in the y-direction only covers the third part of the container, a length of 1 cm in the x-direction limits the area, where a significant grad B exists, and which is therefore the sole thermoelectromagnetically sensitive area, to a region being electrically far from the copper walls. That is to say, the region of strong influence of the copper walls is outside that one, where the source of TEMC $\mathbf{j} \times \mathbf{B}$ is strong – even the overall current distribution in the container is heavily affected by the copper walls, the influence on the TEMC is limited.

Fig. 6 sketches the forces produced by both configurations of the magnetic field (c. f. Figs. 4 and 5) and the assumption of a uniform current between the isothermal walls (c. f. Fig. 1). The coordinate system depicted at the bottom is subsequently used throughout the text. The flow structure that develops under the influence of the force depicted in the left panel is simple: it is a recirculation in the horizontal plane driven by the force acting in the y-direction at the cold wall. The single convection cell rotates clockwise. Also the situation in the right panel is easily understandable. The fluid moves from both the rear and the front wall toward the centre of the box. Recirculation begins when the fluid in the left part of the container gains a velocity component in the $-x$-direction, and that in the right part in the $+x$-direction. The convective pattern will be that of four vortices, in which diagonally opposing cells have the same rolling direction. Because the cell boundaries are not rigid walls, the system with the magnet above the centre is likely the more unstable one. Free boundaries are potential sources of instability in many fluid-dynamic systems.

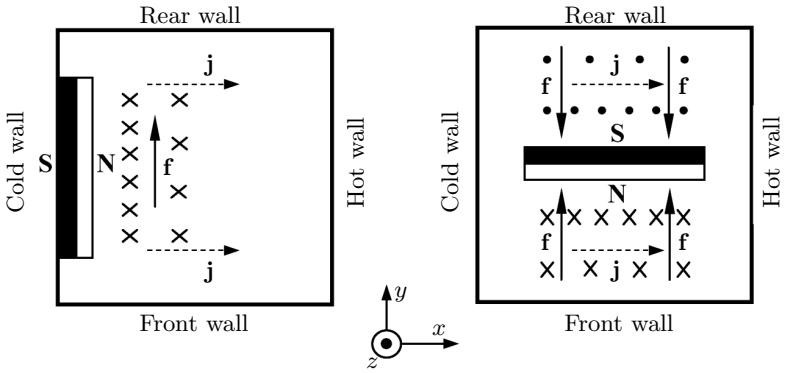

Fig. 6. Top view onto both experimental arrangements investigated in the present work. The thermoelectric current $\mathbf{j}$ in the melt flows in the direction of grad T according to Eq. (3). If the magnet is located above the fluid with its south pole adjacent to the cold wall (left panel), the dominating component of the magnetic field in the liquid layer is B_z. This is because of the ferromagnetic nickel bottom. With the vector of flux density pointing downward, the thermoelectromagnetic body force $\mathbf{f}$ is in the y-direction, being strongest at the magnet and decaying with the increasing distance from the magnet together with B_z. Having the magnet above the centre of the container in the orientation as shown in the right panel, the Lorentz force is directed toward the magnet. $\mathbf{f}$ is strongest in the middle of the magnet and vanishes beyond the ends.

UDV measurements corresponding to the left panel of Fig. 6 are comprised in Fig. 7. While controlling the temperature difference between the hot and cold walls to 30 K, velocity profiles in one of the horizontal directions at a fixed location in the other horizontal direction were sampled for a duration of 120 seconds. Then, the ultrasonic transducer was moved by 1 cm with respect to the second coordinate. This procedure was repeated until the whole area of the container was measured. From the area-wide time-averaged mean values of velocity, a stream function may be computed. The iso-contours in Fig. 7*a* directly correspond to the left panel of Fig. 6 as can be seen from the negative values of the stream function. The single convection cell penetrates the container entirely, while the eye of the vortex

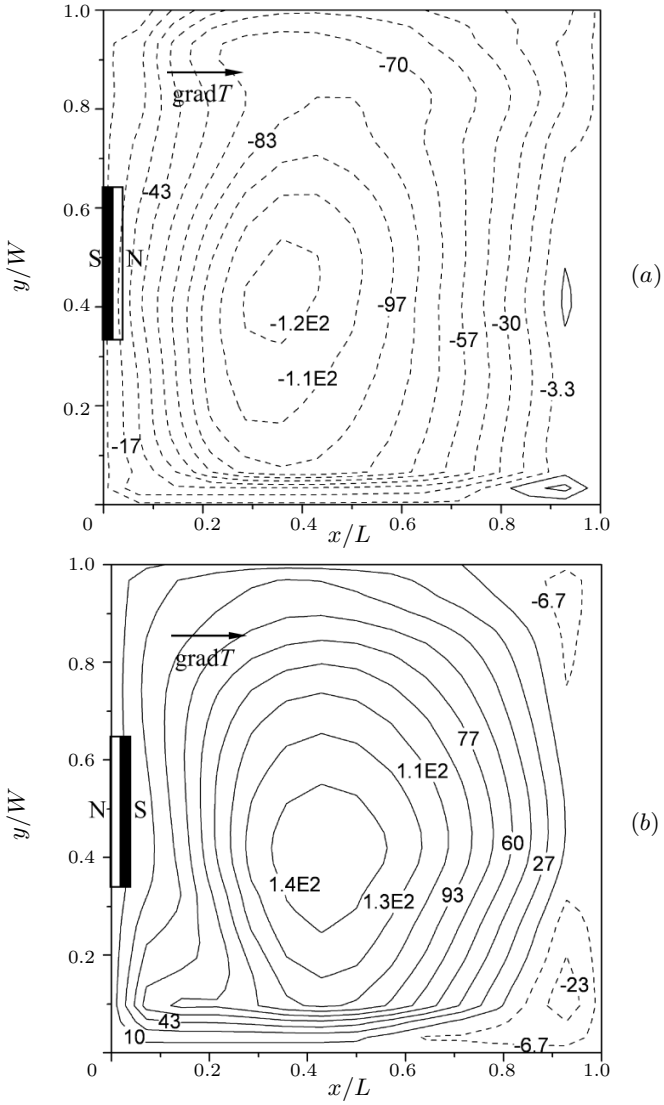

Fig. 7. (*a*) Contour lines of the stream function of the time-averaged flow field for $\Delta T = 30$K. The long side of the magnet is aligned with the cold wall, while the direction of magnetisation is parallel to the temperature gradient. (*b*) Stream function as in (*a*) in the case the direction of magnetisation is reversed. As can be seen from the legends of the iso-lines, the single vortex has an opposing rolling direction, while the absolute value of the stream function does not change within the precision of measurements.

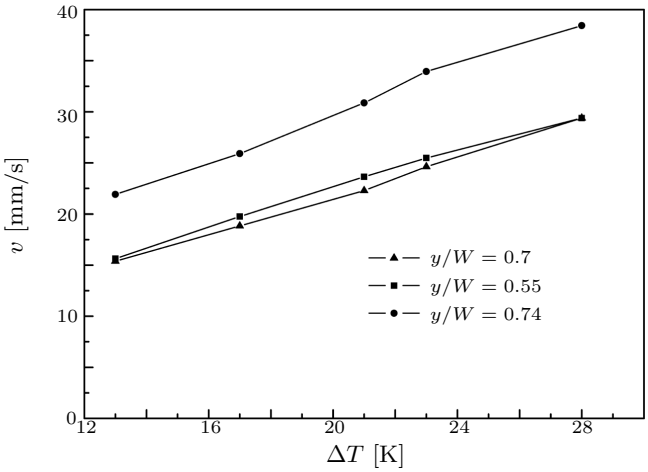

Fig. 8. Mean velocity for the configuration with the magnet at the cold wall in dependence on the temperature difference. The symbols described in the legend denote different positions within the container. The x-coordinate is always close to the cold wall ($x/L = 0.15$), while the y-coordinate is varied.

is moved off the centre toward the source of motion. Such topology is typical for recirculating flows. In Fig. 7*b*, the polarity of the magnet is reversed and the direction of rotation changes from clockwise to counterclockwise, accordingly.

Remaining with time-averaged mean values, Fig. 8 exemplarily shows the dependence on the temperature difference for three positions close to the cold wall. The coordinate ($x = 0.15\,\mathrm{L}, y = 0.55\,\mathrm{W}$) is chosen so as to have the maximum velocity measured there. The small asymmetry indicates that the imperfection of the experimental setup was also small. Both other points are at the same distance from that of highest velocity, and, consequently, the measurements agree very well. In the range up to $\Delta T = 28\,\mathrm{K}$, the measured velocities depend linearly on ΔT, which, in turn, is proportional to the thermoelectromagnetic body force. At half the maximum possible $\Delta T = 25\,\mathrm{K}$, the velocity reaches a value of $v \approx 35\,\mathrm{mm/s}$. Provided that $v \propto \Delta T$ up to $\Delta T = 50\,\mathrm{K}$, a value of 70 mm/s is indeed large compared to 5 mm/s measured for the pure buoyant case for that temperature difference.

Although the flow was relatively stable to the appearance of observation with the naked eye, velocities in the range of several cm/s indicate that the flow is not laminar. A measuring location closer to the eye of the vortex is chosen for closer examination since the ratio of the intensity of velocity fluctuations and the mean velocity are expected to be larger there than in the region of forcing. As can be seen in the time series in Fig. 9, the flow is turbulent.

When the magnet was located above the centre of the container, a convective pattern consisting of four cells developed as expected from the distribution of the thermoelectromagnetic body force above (c. f. Fig. 5). Also in this configuration, both orientations of the magnet, one of which was that the north pole was directed to the front wall leading to a force toward the centre and the other was that the north pole pointed to the rear wall and the force was directed away from the centre, were considered. The corresponding stream functions are to be found in Fig. 10. Again, as in the configuration with the magnet at the cold wall, the vortices change the rolling direction when the direction of magnetisation is inverted.

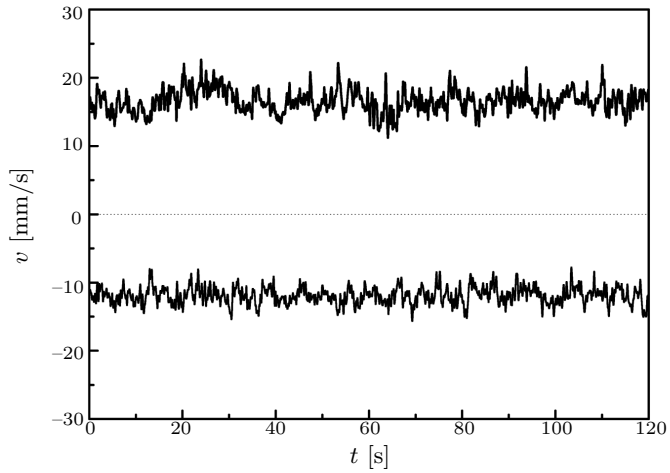

Fig. 9. Time series of the local instantaneous velocity at the position ($x = 0.43\,\mathrm{L}$, $y = 0.37\,\mathrm{W}$) at $\Delta T = 30\,\mathrm{K}$. The upper curve with positive values of the velocity corresponds to the configuration in the left panel of Fig. 6, and the lower one to the right panel.

It could be detected yet from visual observation that, although the temperature difference was 10 K higher than in the case of the single cell, mean velocities decreased distinctly, whereas the turbulence was significantly intensified. Besides the altered topology of the convective pattern and the reduced mean velocities, the turbulence characteristics alone stand for a qualitatively different flow regime. The geometry of the single cell, which is primarily the location of the vortices' eye, was relatively stable. Whatever duration the sampled velocity profiles are averaged, the mean value at any position within the profile does not change much. Only the standard deviation is affected by the characteristic that it approaches asymptotically the turbulence degree, while the part stemming from statistical measuring errors diminishes. In contrast, the four-cell pattern was quite unstable. Mean values obtained from averaging over durations up to 20 seconds even may differ in sign. The flow is characterised by oscillations of the mean eddies, which can be either movement of the vortices' eyes and/or growth and shrinkage of the vortices. Time series for both directions of the magnet are plotted in Fig. 11. Of course, will any averaging tend to a mean value provided a sufficiently long period, over which the average is calculated. Comparison of the time series in Figs. 9 and 11, however, evidences the qualitative difference: the corresponding time scales differ by two orders of magnitude, or even more, and the large-scale pattern *oscillates around a non-existing (zero) mean value.* Intermittence was not observed in the investigated range of the TEMC-driving temperature differences.

6. Conclusion and perspectives. Macroscopically observable thermo-electromagnetic convection (TEMC) was studied in a model experiment. Being generic to a certain extent, the geometry of a square box with a homogeneous temperature gradient between two side walls was chosen in conjunction with employing a small permanent magnet close to the melt surface. The crux of the experiment is that the bottom of the container is made of nickel. Whenever there is a freedom to select the material of structural components being in contact with the melt, the target should be to maximise the thermo-electro motive force (thermo-e.m.f.) with respect to the fluid if a pronounced TEMC is the objective. About 20 μV/K is quite much, this value allowed achieving a time-dependent flow regime even at a moderate temperature difference of 40 K. To the best of our knowledge, turbulent

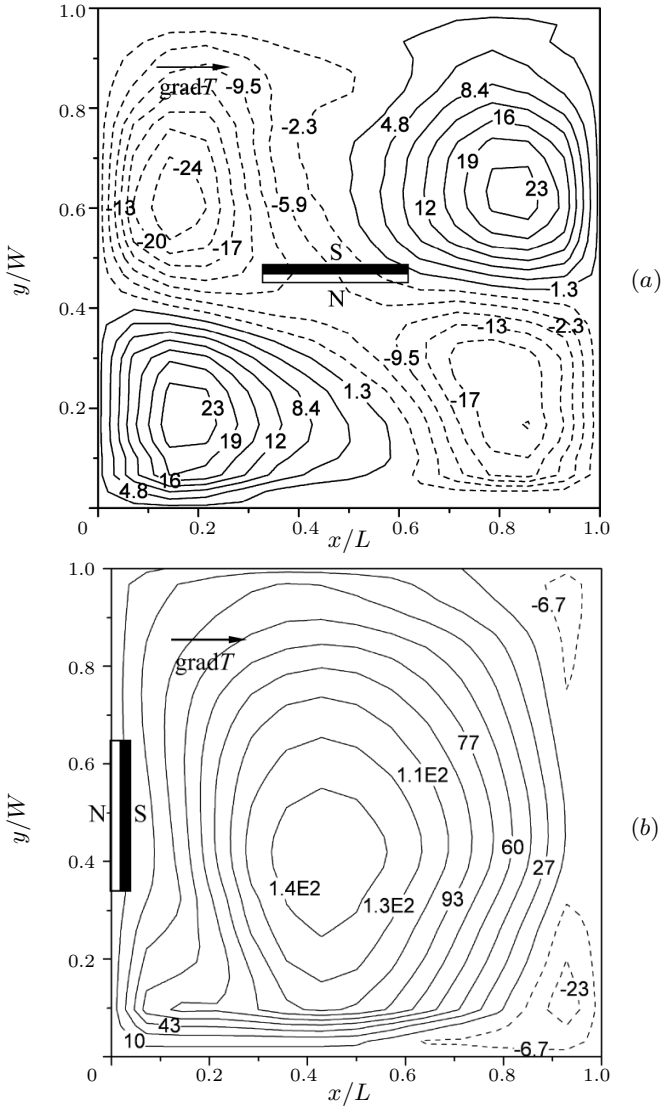

Fig. 10. (*a*) Iso-contours of the stream function calculated from the time-averaged flow field for $\Delta T = 40\,\mathrm{K}$. The convective pattern corresponds to the thermoelectromagnetic force distribution sketched in the right panel of Fig. 6. (*b*) Iso-contours of the stream function as in (*a*) with inverse direction of magnetisation of the permanent magnet.

convection was for the first time observed for the equivalent temperature gradient of only $2.67\,\mathrm{K/cm}$.

As an input parameter to the experiment, the position of the magnet was varied leading to different distributions of the thermoelectrically generated Lorentz force. When the magnet was located close to either isothermal wall with its direction of magnetization parallel to $\mathrm{grad}\,T$, a single vortex developed throughout the whole container, while the flow might be assessed as relatively stable. Moving the magnet to the center modified the topology to four vortices and intensified the velocity fluctuations.

Future work will comprise several modifications of the experimental setup:

• The permanent magnet is replaced by an electromagnet. This firstly allows to increase the absolute value of magnetic flux density. Secondly, the pole shoes

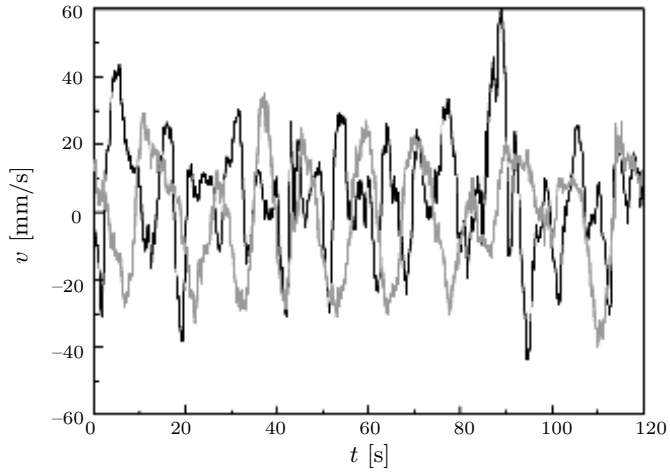

Fig. 11. Instantaneous velocities at the same location as in Fig. 9 at $\Delta T = 40\,\mathrm{K}$. The black line shows the time series when the north pole of the magnet points to the front wall, and the grey line when the magnet is turned by 180°.

are shaped so as to have variation of the flux density only in one direction. This means that the system becomes more generic allowing an easier interpretation of the complex flow pattern.

• Replacing the front and rear copper side walls by walls made of electrically insulating and thermally poor conducting material is advantageous in several concerns. The temperature gradient will be more homogeneous, which also affects the generic nature of the experiment. Moreover, the absolute value is expected to increase. Regarding the current distribution, eliminating the parasitic bypass through these walls will have the effects to make the distribution of thermoelectric currents in the melt more homogeneous and increase the absolute value in the flow driving regions. Again, the generic nature is significantly enhanced.

• Two apparatuses will be produced. Using constantan with $S = -35\mu\mathrm{V/K}$ as the bottom material will increase the thermo-e.m.f. by 50 %, while the disadvantage of having magnetic non-linearity (nickel is ferromagnetic) is removed. A nichrome bottom with $S = 25\mu\mathrm{V/K}$ allows to investigate the *opposite sign* of the TEMC.

Acknowledgement This work is supported by Deutsche Forschungsgemeinschaft in the framework of the collaborative research centre SFB 609 entitled "Electromagnetic Flow Control in Metallurgy, Crystal Growth and Electrochemistry". The authors are grateful to Yurij Plevachuk for preliminary disposal of data on the thermoelectric power of the GaInSn alloy.

REFERENCES

[1] K. F. Schoch. An experimental liquid metal thermoelectric electro-magnetic pump – heat exchanger. *Report No. R56GL94*, General Electric Company, San Jose, CA, USA (1956).

[2] L. B. Vandenberg. Heat exchanger pump. *US patent No. 2,748,710* (1956).

[3] S. R. Rocklin. Thermoelectric pump. *US patent No. 3,116,693* (1964).

[4] M. A. Perlow, H. M. Dieckamp. Thermoelectric pump. *US patent No. 3,288,070* (1966).

[5] J. A. Shercliff. Thermoelectric magnetohydrodynamics. *J. Fluid Mech.*, vol. 91 (1979), pp. 1917–1928.

[6] F. M. Zhargami, J. C. Atwell, S. A. Salamah, U. N. Sinha. Thermoelectric electro-magnetic pump design for the SP-100 reference flight system. *Proc. 24*$^{\text{th}}$ *Intersociety Energy Conversion Engineering Conference*, vol. 2 (1989), pp. 1227–1229.

[7] K. A. Polzin. Liquid metal pump technologies for nuclear surface power. *Proc. Space Nuclear Conference*, Boston, MA, USA (2007).

[8] Y. Y. Khine, J. S. Walker. Thermoelectric magnetohydrodynamics effects during Bridgman semiconductor crystal growth with a uniform axial magnetic field. *J. Cryst. Growth*, vol. 183 (1998), pp. 150–158.

[9] A. Cröll, F. R. Szofran, P. Dold, K. W. Benz, S. L. Lehoczky. Floating-zone growth of silicon in magnetic fields II. Strong static axial fields. *J. Cryst. Growth*, vol. 181 (1998), pp. 554–563.

[10] P. Dold, A. Cröll, K. W. Benz. Floating-zone growth of silicon in magnetic fields I. Weak static axial fields. *J. Cryst. Growth*, vol. 181 (1998), pp. 545–553.

[11] P. Dold, F. R. Szofran, K. W. Benz. Thermoelectromagnetic convection in vertical Bridgeman grown germanium-silicon. *J. Cryst. Growth*, vol. 291 (2006), pp. 1–7.

[12] P. Lehmann, R. Moreau, D. Camel, R. Bolcato. Modification of interdendritic convection in directional solidification by a uniform magnetic field. *Acta Mater.*, vol. 46 (1998), no. 11, pp. 4067–4079.

[13] X. Li, Y. Fautrelle, Z. Ren. Influence of thermoelectric effects on the solid-liquid interface shape and cellular morphology in the mushy zone during the directional solidification of Al-Cu alloys under a magnetic field. *Acta Mater.*, vol. 55 (2007), pp. 3803–3813.

[14] L. A. Gorbunov. Effect of thermoelectromagnetic convection on the production of bulk single-crystals consisting of semiconductor melts in a constant magnetic field. *Magnetohydrodynamics*, vol. 23 (1987), no. 4, pp. 404–408.

[15] M. Kaneda, T. Tagawa, H. Ozoe. Natural convection of liquid metal in a cube with Seebeck effect under a magnetic field. *Int. J. Transp. Phenom.*, vol. 4 (2002), no. 3, pp. 181–191.

[16] K. E. Grew. The variation with temperature of the thermoelectric power of nickel and some copper-nickel alloys. *Phys. Rev.*, vol. 41 (1932), no. 3, pp. 356–363.

[17] A. Bojarevičs, Institute of Physics, Riga, Latvia. *Private communication*, 1995.

[18] Yu. Plevachuk, Ivan Franko National University, Lviv, Ukraine. *Private communication*, 2008.

[19] Y. Takeda. Development of an ultrasound velocity profile monitor. *Nucl. Eng. Des.*, vol. 126 (1991), pp. 277–284.

[20] A. Cramer, C. Zhang, S. Eckert. Local flow structures in liquid metals measured by ultrasonic Doppler velocimetry. *Flow Meas. Instrum.*, vol. 15 (2004), pp. 145–153.

[21] A. Cramer, J. Pal, G. Gerbeth. Experimental investigation of a flow driven by a combination of a rotating and a traveling magnetic field. *Phys. Fluids*, vol. 19 (2007), 118109.

Received 27.1.2008